BUTTERWORTH HEINEMANN

Natural convection from a buried elliptic heat source

George N. Facas
Department of Engineering, Trenton State College, Trenton, NJ, USA

Numerical solutions are presented for the natural convection heat transfer from an elliptic heat source buried beneath a semi-infinite, saturated, porous medium. The surface of the medium is assumed to be permeable. The governing equations for Darcy flow are solved using finite differences. The complicated geometry is handled through the use of a body-fitted curvilinear coordinate system. Results are presented for Ra values ranging from 10 to 200 and ellipse aspect ratio values from 1.0 (circular cylinder) to 0.167. Two body orientations have been considered. The slender orientation yields much higher hear transfer rates (especially at low ellipse aspect ratio values) than the blunt orientation. The numerical simulations indicate that the boundary-layer approximations cannot be employed for low ellipse aspect ratios. In addition, the heat loss does not depend on the burial depth.

Introduction

The problem of free convection from a horizontal circular cylinder buried in a saturated porous medium continues to receive much attention because of its fundamental nature as well as the many engineering applications. This problem arises in power plant steam lines, industrial and agricultural water distribution lines, buried electrical cables, oil and gas distribution lines, and in the storage of nuclear waste.

The early studies that considered the problem of buried cylinders (pipes) and cables assumed the surrounding medium to be purely conductive (see Eckert and Drake 1972; Thiayagarajan and Yovanovich 1978; Bau and Sahdal 1982). However, the assumption that a pure conduction model can be used to calculate the heat losses from a buried pipe may not be valid for high-permeability saturated soils. If the surrounding medium is permeable to fluid motion, the temperature difference between the pipe and the medium gives rise to a natural convection flow. As a result, the total heat transfer from the pipe consists of both conduction as well as convection. Generally, the contribution of natural convection to the heat loss from buried cylinders is as large and, in some cases, larger than the contribution of conduction.

Schrock et al. (1970) and Fernandez and Schrock (1982) carried out experiments and numerical calculations for a cylinder buried beneath a permeable, horizontal surface. Based on their experimental and numerical results, Fernandez and Schrock presented a correlation for the Nusselt number that fitted the data within a standard deviation of 11.4%. Farouk and Shayer (1988) solved the identical problem numerically using a hybrid grid system that involved a polar grid mesh near the cylinder and a Cartesian mesh for the remainder of the flow domain. However, their results were significantly different than the predictions of Fernandez and Schrock, especially at high Ra values. They attributed this to the fact that the boundary condition used along the permeable surface was different in the two studies.

Cheng (1984) considered the steady natural convection about an isothermal cylinder embedded in an infinite saturated porous medium. Approximate closed-form solutions were obtained for the local as well as the average Nusselt number by applying boundary-layer approximations similar to those applied to the classical boundary-layer theory. The applicable boundary-layer equations were solved using both the similarity technique as well as the Pohlhausen integral method. Although the two solutions (in terms of the average Nusselt number) are similar in form, they differ on the numerical constants.

The problem of a cylinder buried beneath a horizontal permeable surface was recently revisited by Facas (1995) who solved the full nonlinear governing equations numerically. The complicated geometry was handled through the use of a body-fitted curvilinear coordinate system. The results presented by Facas (1995) in terms of the local Nusselt number are in excellent agreement with the approximate boundary-layer solution obtained by Cheng (1984) and, also, in excellent agreement with the experimental results presented in terms of the average Nusselt number by Fernandez and Schrock (1982). The work performed by Facas (1995) further showed that the heat loss from a buried pipe can be reduced significantly through the use of a baffle.

Bau (1984a) considered the problem of a pipe buried beneath a permeable as well as an impermeable, horizontal surface. Both the cylinder as well as the medium surface were assumed to be maintained at constant temperature. For low Rayleigh numbers, an analytical solution was obtained for both permeable and impermeable medium surfaces through the use of regular perturbation expansions. Based on the analytical solution that was obtained for the flow and temperature fields, a correlation for the Nusselt number was presented for the impermeable case, which is valid up to an effective Rayleigh number of 60. It was further shown that an optimal burial depth exists for the impermeable case for which the heat losses from the pipe are minimized. Facas (1994) considered the problem of a hot pipe buried beneath an

Address reprint requests to Prof. G. N. Facas, Department of Engineering, Trenton State College, Hillwood Lakes, CN 4700, Trenton, NJ 08650-4700.

Received 27 January 1995; accepted 14 July 1995

Int. J. Heat and Fluid Flow 16: 519–526, 1995

655 Avenue of the Americas, New York, NY 10010

0142-727X/95/$10.00
SSDI 0142-727X(95)00059-Y

impermeable surface of a semi-infinite, saturated porous medium with two baffles attached on the pipe's surface. Results were presented for a range of Rayleigh numbers, burial depths, and baffle lengths, respectively. His analysis showed that substantial energy savings can be realized if baffles are used.

Recently, Pop et al. (1992) presented numerical solutions to the boundary-layer equations for steady-state free convection from cylinders of elliptic cross section embedded in a fluid-saturated porous medium. Uniform temperature as well as uniform heat flux boundary conditions were considered at the cylinder surface. Moreover, two body orientations were considered: one where the major axis is horizontal (blunt orientation) and the other where it is vertical (slender orientation). Numerical results were presented for a number of aspect ratios for both the blunt as well as the slender orientation. Based on the numerical results obtained, Pop et al. concluded that for the uniform wall temperature case, the blunt orientation yields higher heat transfer rates; whereas, the opposite holds true for the uniform wall heat flux case.

The present study deals with the natural convection over an elliptic heat source buried in a semi-infinite, saturated, permeable medium, the surface of which is assumed to be horizontal and permeable to fluid flow. To the best of the author's knowledge, the solution to the full nonlinear equations that govern the free convection over a body of elliptic cross section is not available in the literature. The geometry and configuration involved in this study is depicted schematically in Figure 1. The complicated geometry is handled through the use of a body-fitted curvilinear coordinate system. The solution to the fluid flow and temperature field has been obtained numerically using finite differences.

Mathematical formulation

The problem considered in this study is an elliptic heat source buried a distance h beneath a horizontal permeable surface of a semi-infinite, saturated, porous medium, as shown in Figure 1. Two geometric orientations are considered: (1) the major axis is horizontal and perpendicular to the gravity vector (blunt orientation); and (2) the major axis is vertical and parallel to the gravity vector (slender orientation). For both orientations, the surface of the elliptic source is assumed to be maintained at a constant temperature T_b.

For low Ra values, the dimensionless governing equations for steady, two-dimensional (2-D) natural convection with the Boussinesq, Darcy flow and negligible inertia approximations are as follows:

$$\nabla^2\psi^* = -\mathrm{Ra}\,\theta_{x'}, \tag{1}$$

$$\nabla^2\theta = \psi^*_{y'}\theta_{x'} - \psi^*_{x'}\theta_{y'}, \tag{2}$$

where

$$\mathrm{Ra} = \frac{g\rho_o\rho_f c_f\beta_f bK\Delta T}{\lambda'\mu};\quad \Delta T = T_b - T_o;\qquad \theta = \frac{T - T_o}{T_b - T_o} \tag{3}$$

$$u' = \psi^*_{y'};\qquad v' = -\psi^*_{x'},\qquad \psi^* = \frac{c_f\psi}{\lambda'};\qquad x' = \frac{x}{b},\qquad y' = \frac{y}{b} \tag{4}$$

and

$$\lambda' = \lambda_s(1-\phi) + \lambda_f\phi \tag{5}$$

The solution of Equations 1 and 2 with appropriate boundary conditions gives the desired distribution for ψ^* and θ.

Boundary conditions

The problem is assumed to be symmetric about the vertical axis and, as a result, only half of the flow domain is considered in this analysis. Moreover, because it is very difficult to treat an infinite domain numerically, the physical domain will be truncated by assuming that the two far boundaries at infinite x' and negative infinite y' are at a large distance (w/b) and (d/b) away from the center of the ellipse, respectively. Appropriate values for (w/b) and (d/b) (lead to solutions that are independent of the value set for these two quantities) can be selected only through numerical experimentation.

At the elliptic body surface the following boundary condition is used: $\theta = 1$; $\psi* = 0$, @ $(b/a)^2x'^2 + y'^2 = 1$ or $x'^2 + (b/a)^2y'^2 = 1$; whereas, along the symmetry axis, $\theta_{x'} = \psi^*_{y'} = \psi^* = 0$ $x' = 0$.

If the two far fields are set sufficiently far away from the source, then the velocity component in the direction parallel to each surface can be assumed to be negligible. Thus, the boundary

Notation

a	major axis
b	minor axis
c	specific heat
f	ellipse aspect ratio ($f = b/a$)
$\mathbf{g}$	gravity vector
h	burial depth
$\hat{h}$	convective heat transfer coefficient
K	permeability
Nu	Nusselt number, Equation 12
Ra	Rayleigh number, Equation 3
T	temperature
x, y	Cartesian coordinates, Figure 1
x', y'	dimensionless Cartesian coordinates, Equation 4
u', v'	dimensionless Cartesian velocity components

Greek

β	volumetric thermal expansion coefficient
γ	circumferential (angle) coordinate, Figure 1
θ	dimensionless temperature
λ	thermal conductivity
μ	kinematic viscosity
ρ	density
ϕ	porosity
ψ	stream function
ψ^*	dimensionless stream function
ξ, η	body-fitted coordinates

Subscripts

b	heat source surface
f	fluid
s	solid
o	reference state

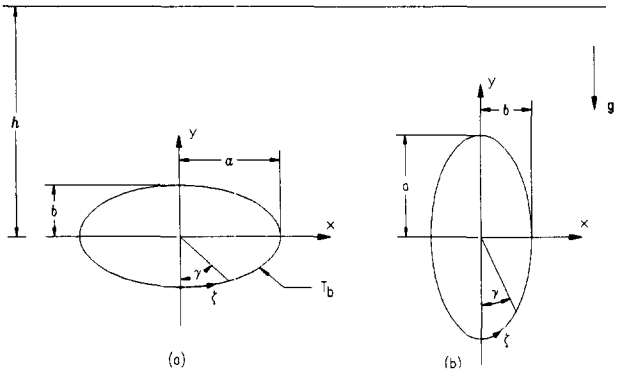

Figure 1 Geometry and configuration: (a) blunt; (b) slender

condition for the stream function at the bottom surface ($y' = -d/b$) becomes $\psi^*_{y'} = 0$ and at the far right surface ($x' = w/a$)$\psi^*_{x'} = 0$.

Zero gradient temperature boundary conditions were considered at these two far surfaces: $\theta_{y'} = 0$ at $y' = -d/b$, and $\theta_{x'} = 0$ at $x' = w/b$. The least restrictive condition that can be imposed along the top permeable surface is that of a constant pressure. A constant pressure condition would exist if either a standing liquid or a second porous medium (with a larger permeability) overlies the porous layer of interest. Thus, for the case of a constant pressure, a balance of momentum in the x-direction yields at the top permeable surface $u' = \psi^*_{y'} = 0$.

Specifying the thermal boundary condition along the top permeable surface is not as straightforward. For the limiting case of a circular cylinder buried beneath a permeable surface, a number of different temperature boundary conditions have been imposed by the various investigators that have considered this problem to date. Fernandez and Schrock (1982) used a condition similar to that used in transpiration cooling that accounts for the convective flow of energy through the surface as well as conduction to the surface and convection to the overlaying water. Bau (1984a) assumed a constant temperature condition. The assumption of a constant temperature may be, however, difficult to physically realize especially at high Rayleigh numbers. Facas (1995) imposed a zero temperature gradient condition that implies that the heat transfer through the permeable surface to the overlying liquid layer is primarily by convection. The results presented by Facas for a circular cylinder buried beneath a permeable surface are in very good agreement (within 10%) with the experimental and numerical results presented for the same geometry by Fernandez and Schrock and in excellent agreement with the analytical results presented for a cylinder buried in an infinite porous medium by Cheng (1984). It is important to note here that the results (obtained with the correlation) presented by Fernandez and Schrock are always larger by about 10% than the results given by Facas (1995). However, based on the few experimental data that were presented for a cylinder of large aspect ratio (actual experimental data are shown for $L/D = 76.7$), it appears that the correlation given by Fernandez and Schrock overestimates the heat transfer for the Rayleigh range considered by Facas (1995) (see Figure 5 of Fernandez and Schrock). When this observation is taken into consideration, it is clear that the agreement between the numerical data presented by Facas (1995) and the experimental results of Fernandez and Schrock is excellent. Consequently, it is argued here that a zero temperature gradient condition can be specified along the entire top permeable surface without affecting the ability to accurately predict the heat transfer from the source. Thus, the temperature boundary condition at the top permeable surface was set to $\theta_{y'} = 0$.

Boundary-fitted coordinates

As previously noted, a truncated rectangular domain is used to approximate the flow domain. A Cartesian grid could, in principle, be adopted with the present problem, as it is often done with conduction problems. However, in order to obtain accurate solutions with problems that involve convection, it is advantageous to have all rigid surfaces coincide with a surface on which one of the coordinates is constant. Following Facas (1994), a new body-fitted curvilinear coordinate system is introduced such that the various surfaces coincide with constant values of ξ and η, as shown in Figure 2. From the various techniques available, the partial differential equation (PDE) method presented by Thompson et al. (1982) is chosen. Briefly, the transformation relations for the mapping are obtained by solving the following nonlinear system of partial differential equations (from this point on the nondimensional spatial coordinates x' and y' are referred to as simply x and y; i.e., the primes are dropped):

$$\alpha_1 x_{\xi\xi} - 2\alpha_2 x_{\xi\eta} + \alpha_3 x_{\eta\eta} + \mathbf{J}^2(Px_\xi + Qx_\eta) = 0 \tag{6}$$

$$\alpha_1 y_{\xi\xi} - 2\alpha_2 y_{\xi\eta} + \alpha_3 y_{\eta\eta} + \mathbf{J}^2(Py_\xi + Qy_\eta) = 0 \tag{7}$$

where

$$\alpha_1 = x_\eta^2 + y_\eta^2, \qquad \alpha_2 = x_\xi x_\eta + y_\xi y_\eta, \qquad \alpha_3 = x_\xi^2 + y_\xi^2$$

$$\mathbf{J} = x_\xi y_\eta - x_\eta y_\xi \tag{8}$$

and P and Q are functions of ξ and η. Their function is to control the spacing between adjacent ξ and η grid lines, respectively. In this study, P and Q were set to

$$P = 0$$

$$Q = -z_1\{\mathrm{sgn}(\eta - \eta_1)\exp[-z_2(\eta - \eta_1)] + \mathrm{sgn}(\eta - \eta_2)\exp[-z_2(\eta_2 - \eta)]\} \tag{9}$$

where z_1 and z_2 are constants.

The solution to Equations 6 and 7 was obtained iteratively using central differences. An example of the resulting grid is shown in the physical plane in Figure 2. The computational plane consists of the rectangle $\xi_1 \le \xi \le \xi_2$ and $\eta_1 \le \eta \le \eta_2$.

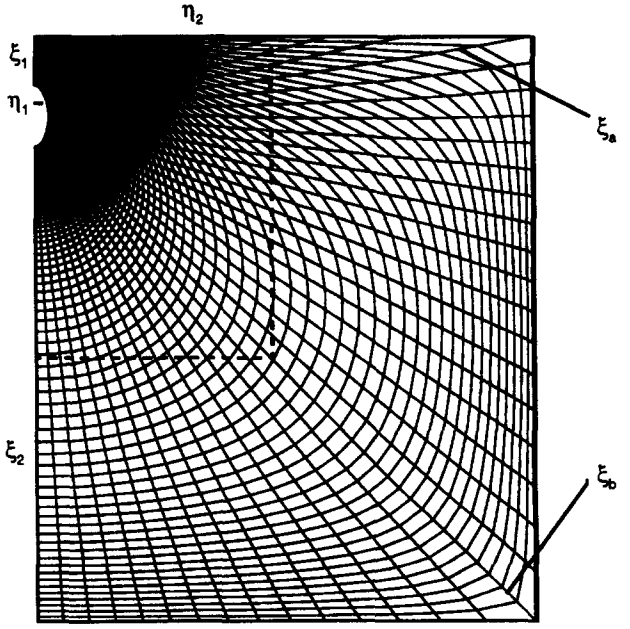

Figure 2 An example of the body-fitted curvilinear coordinates ($f = 0.5$, $h/b = 8$, $w/b = d/b = 38$)

When the governing Equations 1 and 2 and corresponding boundary conditions are also transformed into the new coordinate system (ξ, η) the resulting equations become:

$$\alpha_1\psi^*_{\xi\xi} - 2\alpha_2\psi^*_{\xi\eta} + \alpha_3\psi^*_{\eta\eta} + \mathbf{J}^2\left(P\psi^*_\xi + Q\psi^*_\eta\right) = -\mathrm{Ra}\mathbf{J}\left(y_\eta\theta_\xi - y_\xi\theta_\eta\right) \quad (10)$$

$$\alpha_1\theta_{\xi\xi} - 2\alpha_2\theta_{\xi\eta} + \alpha_3\theta_{\eta\eta} + \mathbf{J}^2\left(P\theta_\xi + Q\theta_\eta\right) = \mathbf{J}\left(\psi^*_\eta\theta_\xi - \psi^*_\xi\theta_\eta\right) \quad (11)$$

and the corresponding boundary conditions become as follows:

Heat source surface:

$$\theta = 1, \quad \psi^* = 0 \quad \text{at} \quad \xi_1 \le \xi \le \xi_2; \quad \eta = \eta_1 \quad (12a)$$

Top permeable surface:

$$x_\eta\psi^*_\xi - x_\xi\psi^*_\eta = x_\eta\theta_\xi - x_\xi\theta_\eta = 0 \quad \text{at} \quad \xi_1 \le \xi \le \xi_2; \quad \eta = \eta_2 \quad (12b)$$

Symmetry axis:

$$\psi^* = \theta_\xi = 0 \quad \text{at} \quad \xi = \xi_1; \quad \eta_1 \le \eta \le \eta_2$$

$$\psi^* = \theta_\xi = 0 \quad \text{at} \quad \xi = \xi_2; \quad \eta_1 \le \eta \le \eta_2 \quad (12c)$$

Far-right surface:

$$y_\eta\psi^*_\xi - y_\xi\psi^*_\eta = y_\eta\theta_\xi - y_\xi\theta_\eta = 0 \quad \text{at} \quad \xi_a \le \xi \le \xi_b; \quad \eta = \eta_2 \quad (12d)$$

Far-bottom surface:

$$x_\eta\psi^*_\xi - x_\xi\psi^*_\eta = x_\eta\theta_\xi - x_\xi\theta_\eta = 0 \quad \text{at} \quad \xi_b \le \xi \le \xi_2; \quad \eta = \eta_2 \quad (12e)$$

The solution of Equations 10 and 11 subject to the conditions specified by Equation 12 yields the desired distribution for ψ^* and θ.

Heat transfer

The local Nusselt number along the source surface is defined as follows:

$$\mathrm{Nu} = \frac{\hat{h}b}{\chi} = -\left(\frac{\partial\theta}{\partial n}\right)_{x^2+(b/a)^2y^2=1 \text{ or } (b/a)^2x^2+y^2=1} \quad (13)$$

where n represents the direction normal to the heat source surface. Because the heat source surface in the computational domain is represented by a constant η-line, the directional derivative shown in Equation 13 expressed in terms of ξ and η becomes, Thompson et al. (1979)

$$\mathrm{Nu}(\xi, \eta_1) = -\left(\frac{\partial\theta}{\partial\eta}\right)_{\eta=\eta_1} = -\left(\alpha_3\frac{\partial\theta}{\partial\eta} - \alpha_2\frac{\partial\theta}{\partial\xi}\right)_{\eta=\eta_1} \Big/ J\sqrt{\alpha_3} = -\left(\frac{\sqrt{\alpha_3}}{J}\frac{\partial\theta}{\partial\eta}\right)_{\eta=\eta_1} \quad (14)$$

The average Nusselt number, $\overline{\mathrm{Nu}}$ at the elliptic heat source surface is given by

$$\overline{\mathrm{Nu}} = \frac{1}{\xi_2 - \xi_1}\int_{\xi_1}^{\xi_2}\mathrm{Nu}(\xi, \eta_1)\, d\xi \quad (15)$$

Numerical solution

The solution to Equations 10 and 11 subject to the boundary conditions specified by Equation 12 is obtained numerically using finite differences. Central differences are used to approximate the diffusive terms; whereas, the upwind differencing scheme was introduced with the convective terms (Roache 1976). The resulting algebraic equations were solved iteratively using the method of overrelaxation (S.O.R.). The iterative procedure was terminated when the following relative convergence criterion was satisfied at every grid point.

$$\left|\frac{\psi^{n+1}_{ij} - \psi^n_{ij}}{\psi^n_{ij}}\right|, \left|\frac{\theta^{n+1}_{ij} - \theta^n_j}{\theta^n_{ij}}\right| \le 5 \times 10^{-5}$$

where the superscript n denotes the iteration performed.

To ensure that the numerical code is validated, the convection problem within two concentric, horizontal cylinders for which solutions are available was solved. The results obtained using the present code are in good agreement with those of Caltagirone (1976), Facas and Farouk (1983), Bau (1984b), and Rao et al. (1987); see Facas (1995) for further details. To validate further the numerical model, the solutions obtained with the present model for a circular cylinder buried beneath a permeable surface were compared (in terms of the average Nusselt number) with the experimental and numerical results presented for the same problem by Fernandez and Schrock (1982); see Facas (1995) for further details. Furthermore, the local as well as the average Nusselt number distribution predicted with the present model for a circular cylinder was also compared to the analytical results presented for a cylinder buried in a infinite porous medium by Cheng (1984), see Figure 7.

The numerical results for the problem under consideration will, in general, be sensitive to the values set for (w/b) and

Table 1 Effect of grid size on the accuracy of the solution ($h/b = 8$, $f = 1$, $w/b = d/b = 38$)

Ra		Grid Size (ξ, η) *				
		60 × 60	60 × 90	60 × 120	Cheng (1984)	Fernandez and Schrock (1982)
50	$\overline{\mathrm{Nu}}$	2.974	3.031	3.057	2.828	3.200
	ψ^*_{max}	−28.28	−28.11	−28.03		
100	$\overline{\mathrm{Nu}}$	4.165	4.226	4.255	4.000	4.569
	ψ^*_{max}	−42.95	−42.52	−42.32		

* The two constants z_1 and z_2 in Equation 9 are same for all three grid sizes

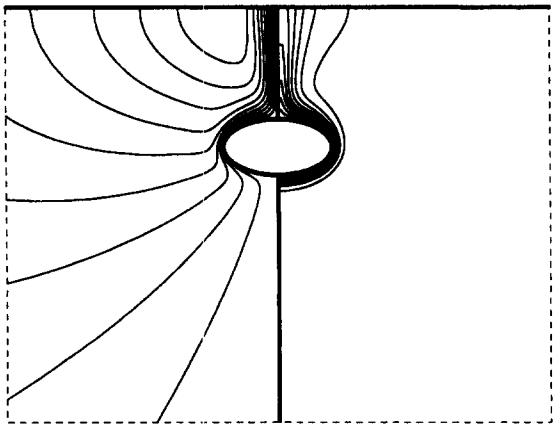

Figure 3 Uniformly spaced streamlines (left-hand side) and isotherms (right-hand side) corresponding to the blunt orientation for $f = 0.5$, $h/b = 5$, Ra = 100 ($\Delta\psi^* = 3.62$, $\Delta\theta = 0.1$)

(d/b). As a result, a considerable effort has been directed to select values for (w/b) and (d/b) so that the solution is independent of the value selected for these two quantities. Based on the results presented by Facas (1995), the minimum value considered in this analysis for (w/b) and (d/b) was about 38 and, in some cases, values as large as 57 were used [see Facas (1995) for further details on the effect of w/b and d/b on the solution).

A considerable effort in this study was also directed toward determining the minimum number of grid points required to obtain solutions that are grid independent. For $(h/b) \leq 8$, a grid size of 60×90 was found to yield solutions that are reasonably grid independent and in very good agreement with the experimental and numerical results presented for a pipe buried beneath a permeable surface by Fernandez and Schrock (1982) and Cheng (1984); see Table 1.

Three-point finite differences were used to evaluate the local Nusselt number. The average Nusselt number was evaluated using Simpson's rule. All computations were carried out on a 486 personal computer.

Results and discussion

Numerical solutions have been obtained for the blunt as well as the slender orientation for Rayleigh numbers (based on the minor

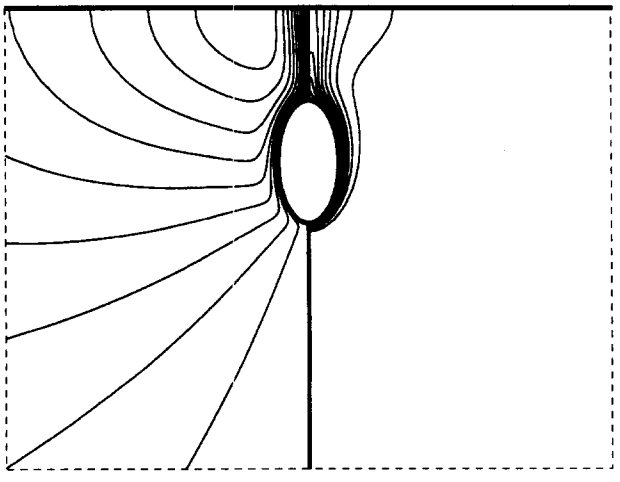

Figure 4 Uniformly spaced streamlines (left-hand side) and isotherms (right-hand side) corresponding to the slender orientation for $f = 0.5$, $h/b = 5$, Ra = 100 ($\Delta\psi^* = 3.91$, $\Delta\theta = 0.1$)

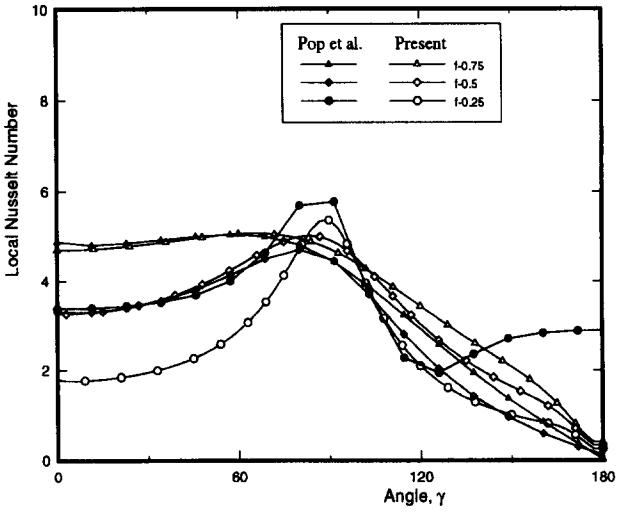

Figure 5 Local Nusselt number distributions corresponding to the blunt orientation, $h/b = 8$ and Ra = 100

axis) in the range of 10 to 200; burial depths (h/b) varying from 4 to 8; and ellipse aspect ratios $(f = b/a)$ ranging from 0.167 to 1.0 (circular cylinder).

The flow and temperature field associated with an elliptic heat source buried at a depth $h/b = 5$, aspect ratio $f = 0.5$, and Ra = 100 is depicted in Figures 3 and 4 for the blunt and slender orientation respectively. As it is illustrated in Figures 3 and 4, the fluid flow is basically upward; the fluid adjacent to the source becomes hotter, and it begins to rise until it reaches the top permeable surface through which it is finally discharged to the surroundings. The isotherm patterns indicate a maximum temperature gradient near $\gamma = 90°$ for the blunt orientation and $\gamma = 0°$ for the slender orientation, respectively. The streamline plots show that the fluid is accelerating from a low-velocity point below the ellipse to a high-velocity region above the ellipse. Clearly, at Ra = 100, the streamline and isotherm plots indicate the existence of a thin thermal boundary layer. Also, some refilling seems to occur through the upper permeable surface. It is important to note that the physical domain shown in Figures 3 and 4 represents only a small portion (region near the heat source bounded by the dashed line in Figure 2) of the domain that was

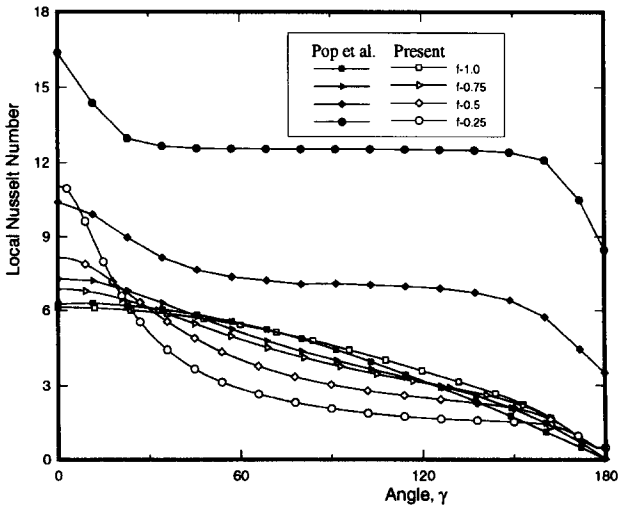

Figure 6 Local Nusselt number distributions corresponding to the slender orientation, $h/b = 8$ and Ra = 100

considered in the analysis in order to be able to show details near the source.

In Figures 5 and 6 the solutions obtained in terms of the local Nusselt number are compared to the numerical solutions obtained (converted to the notation used by this author) from the corresponding boundary-layer equations to this problem by Pop et al. (1992). Clearly, for ellipse aspect ratios ($f = b/a$) in the range of 0.75 to 1.0, the solutions presented by the two studies are in good agreement for both the blunt as well as the slender orientation. However, as the ellipse aspect ratio decreases to 0.5, the boundary-layer solution corresponding to the slender orientation "breaks" the trend that was established at the slightly higher aspect ratios and yields much larger Nusselt number values. It is important to note here that the heat transfer for the problem under consideration is a very weak function of burial depth, as it shown later. As a result, the comparison with the results presented by Pop et al. is valid, although their results correspond to a cylinder buried in an infinite domain. The value obtained for the average Nusselt number from the boundary-layer solution increases even more with decreasing ellipse aspect ratio values, as it is evident from the solution corresponding to $f = 0.25$. It is interesting to observe that for the blunt orientation, the boundary-layer solutions show no dependence (in terms of the local Nusselt number) on the aspect ratio for the lower part of the ellipse once the aspect ratio value is less than 0.5. It is also interesting to note that the boundary-layer solution corresponding to the blunt orientation and $f = 0.25$ indicates that the local Nusselt number reaches a maximum near $\gamma = 90°$, proceeds to achieve a minimum along the top portion of the ellipse, at which point it reverses direction and begins to increase once again. Clearly, these findings are not confirmed by the solutions obtained in this study.

Because large discrepancies exist at low ellipse aspect ratios between the solutions obtained in this study and the boundary-layer solutions presented by Pop et al. (1992) for the slender orientation, two limiting cases have been considered in order to validate the present model. The first case corresponds to a circular cylinder ($f = 1.0$); whereas, the second corresponds to that of a vertical heated plate. For both of these limiting cases, Cheng (1984) presented similarity solutions. As the aspect ratio decreases, the local Nusselt number distribution for a slender ellipse should, in the limit, approach the local Nusselt number distribution for a heated vertical wall. For a heated vertical wall, the local Nusselt number distribution is given by Cheng (1984) as follows:

$$\mathrm{Nu}_x = 0.444\sqrt{\mathrm{Ra}_x}, \qquad x \geq 0 \tag{16}$$

where x here is measured from the leading point of the vertical plate. Thus, an approximation for the local Nusselt number distribution corresponding to the slender case can be written in terms of Ra (defined in terms of b) as follows:

$$\mathrm{Nu}(\gamma) = \frac{\hat{h}b}{\lambda} \approx 0.444\sqrt{\mathrm{Ra}(b/\zeta)}, \qquad \zeta \geq 0 \tag{17}$$

where ζ represents the arc length (as shown in Figure 1), and its value is obtained from the elliptic integral:

$$\zeta = a\int_0^{\gamma}\sqrt{(1 - e^2\sin^2\varphi)}\,\mathrm{d}\varphi;\; e^2 = \frac{a^2 - b^2}{a^2} \tag{18}$$

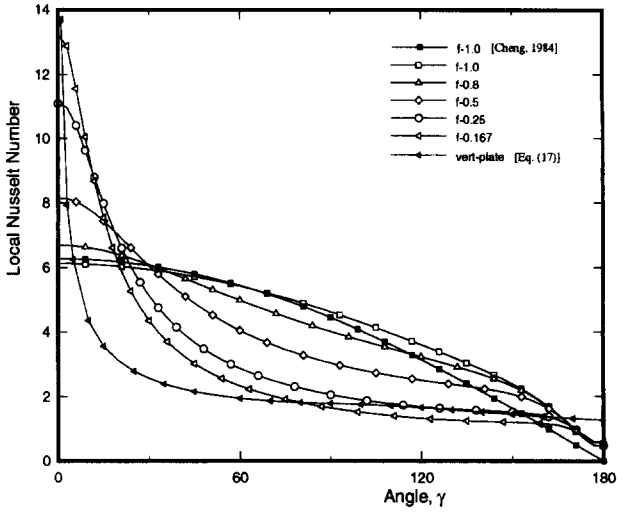

Figure 7 Local Nusselt number distributions corresponding to the slender orientation, $h/b = 8$ and $\mathrm{Ra} = 100$

Table 2 Average Nusselt number as a function of Ra, ellipse aspect ratio f, and body orientation; $h/b = 8$

Ra	$f = b/a$	Blunt orientation	Slender orientation
10	1.0	1.300	1.300
	0.8	1.219	1.227
	0.667	1.115	1.211
	0.5	1.058	1.098
50	1.0	3.031	3.031
	0.8	2.826	2.913
	0.667	2.643	2.792
	0.5	2.345	2.615
100	1.0	4.226	4.226
	0.8	3.953	4.049
	0.75	3.794	4.001
	0.667	3.621	3.911
	0.5	3.221	3.687
	0.25	2.347	3.146
	0.167	–	2.825
150	1.0	5.127	5.127
	0.8	4.774	5.009
	0.5	3.859	4.530
200	1.0	5.879	5.879
	0.8	5.470	5.762
	0.5	4.399	5.220

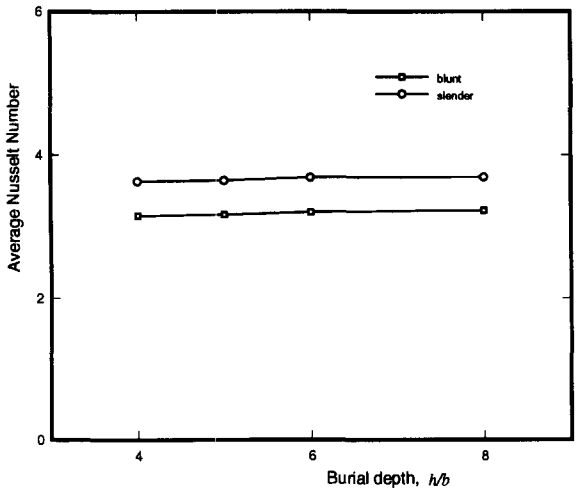

Figure 8 Average Nusselt number as a function of h/b, Ra = 100, $f = 0.5$

Figure 7 shows the local Nusselt number distribution predicted by Equation 17 (with $f = b/a = 0.167$ and Ra = 100), the similarity solution presented by Cheng (1984) for the case of a circular cylinder, and the solutions that were obtained in this study for a number of ellipse aspect ratio values. As can be seen, the solution corresponding to $f = 0.167$ is approaching the approximate solution given by Equation 17, thus validating the predictions of this study. Based on this, it is argued that the numerical solutions to the boundary-layer equations presented for the problem under consideration by Pop et al. (1992) are not valid for ellipse aspect ratios less than 0.5 for the blunt orientation and 0.75 for the slender orientation.

Average Nusselt number results as a function of burial depth (h/b) are shown in Figure 8 for Ra = 100 and $f = 0.5$ for both the blunt as well as the slender orientation. Clearly, from Figure 8 it can be seen that the heat transfer for both the blunt as well as the slender orientation is a very weak function of the burial depth. Although not shown here, similar conclusions about the dependence of the heat transfer on burial depth were drawn for all Ra and f values considered in this study. It is important to note here that this finding is consistent with the experimental findings of Fernandez and Schrock (1982) for a buried cylinder. Average Nusselt number values associated with an elliptic heat source buried beneath a permeable surface a distance $h/b = 8$ are tabulated in Table 2 for a number of Ra and f values for both the blunt as well as the slender orientation. The results indicate

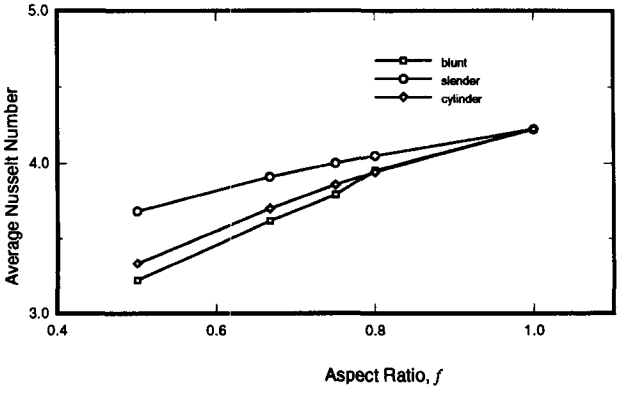

Figure 9 Average Nusselt number as a function of f, Ra = 100, $h/b = 8$

that the slender orientation yields much higher overall heat transfer rates (especially at low f values) than the blunt orientation, which is the opposite of the conclusion drawn by Pop et al. (1992).

Finally, in Figure 9 the average Nusselt number corresponding to Ra = 100 and $h/b = 8$ is plotted as a function of ellipse aspect ratio f. Also plotted in this figure is the average Nusselt number associated with a circular cylinder with the same surface area as the corresponding ellipses. Clearly, the slender orientation yields always higher heat transfer rates than a cylinder; whereas, the heat transfer rate corresponding to the blunt case is slightly lower than that from a cylinder.

Conclusion

A numerical investigation has been performed to solve for the flow and temperature fields for a heat source with an elliptic cross section buried in a saturated porous medium the surface of which is assumed to be permeable to fluid flow. Results are presented for a range of Rayleigh numbers, ellipse aspect ratios, burial depths, and two body orientations. For high-aspect ratio values, the present results in terms of the local and average Nusselt number are in good agreement with the solution to the boundary-layer equations available in the literature. Based on the numerical solutions presented by Pop et al. (1992), the boundary-layer assumptions do not yield valid solutions for low ellipse aspect ratio values. Moreover, it has been shown that the heat transfer from the elliptic source does not really depend on burial depth. In addition, the slender orientation yields much higher heat transfer rates than the blunt orientation.

Acknowledgments

This work was partially supported by a FIRSL research award administered by Trenton State College. The author expresses his appreciation to the College.

References

Bau, H. H. 1984a. Convective heat losses from a pipe buried in a semi-infinite porous medium. *Int. J. Heat Mass Transfer*, **27**, 2047–2056

Bau, H. H. 1984b. Thermal convection in a horizontal, eccentric annulus containing a saturated porous medium — An extended perturbation expansion. *Int. J. Heat Mass Transfer*, **27**, 2277–2287

Bau, H. H. and Sadhal, S. S. 1982. Heat losses from a fluid flowing in a buried pipe. *Int. J. Heat Mass Transfer*, **25**, 1621–1629

Caltagirone, J. P. 1976. Thermoconvective instabilities in a porous medium bounded by two concentric horizontal cylinders. *J. Fluid Mech.*, **76**, 337–362

Cheng, P. 1984. Natural convection in a porous medium: External flows. Paper presented at NATO Advanced Study Institute, July 16–27

Eckert, E. R. G. and Drake, R. M. 1972. *Analysis of Heat and Mass Transfer*. McGraw-Hill, New York

Facas, G. N. and Farouk, B. 1983. Transient and steady-state natural convection in a porous medium between two concentric cylinders. *J. Heat Transfer*, **105**, 660–663

Facas, G. N. 1994. Reducing the heat transfer from a hot pipe buried in a semi-infinite, saturated, porous medium. *J. Heat Transfer*, **116**, 473–476

Facas, G. N. 1995. Natural convection from a buried pipe with external baffles. *Num. Heat Transfer, Part A*, **27**, 595–609

Farouk, B. and Shayer, H. 1988. Natural convection around a heated cylinder in a saturated porous medium. *J. Heat Transfer*, **110**, 642–648

Fernandez, R. T. and Schrock, V. E. 1982. Natural convection from cylinders buried in a liquid-saturated porous medium. *Proc. Int. Heat Transfer Conference*, Munich, Germany, **72**, 335–340

Pop, I., Kumari, M. and Nath, G. 1992. Free convection about cylinders of elliptic cross section embedded in a porous medium. *Int. J. Eng. Sci*, **30**, 35–45

Rao, Y. F., Fukuda, K. and Hasegawa, S. 1987. Steady and transient analyses of natural convection in a horizontal porous annulus with the Galerkin method. *J. Heat Transfer*, **109**, 919–927

Roache, P. J. 1972. *Computational Fluid Dynamics*. Hermosa Publishers, Albuquerque, NM

Schrock, V. E., Fernandez, R. T. and Kesavan, K. 1970. Heat transfer from cylinders embedded in a liquid-filled porous medium. *Proc. Int. Heat Transfer Conference*, Paris, France, **VII**, CT 3.6

Thiyagarajan, R. and Yovanovich, M. M. 1974. Thermal resistance of a buried cylinder with constant flux boundary condition. *J. Heat Transfer*, **96**, 249–250

Thompson, J. F., Warsi, Z. U. A. and Mastin, C. W. 1982. Boundary-fitted coordinate system for numerical solution of partial differential equations — A review. *J. Comp. Physics*, **47**, 1–108

Thompson, J. F., Thames, F. C. and Mastin, C. W. 1979. Boundary-fitted curvilinear coordinate systems for solution of partial differential equations on fields containing any number of arbitrary two-dimensional bodies. NASA, CR-2729